nature nanotechnology

Article

https://doi.org/10.1038/s41565-023-01397-0

Engineering metal oxidation using epitaxial strain

In the format provided by the authors and unedited

Supplementary Information

Table of Contents:

Figure S1:

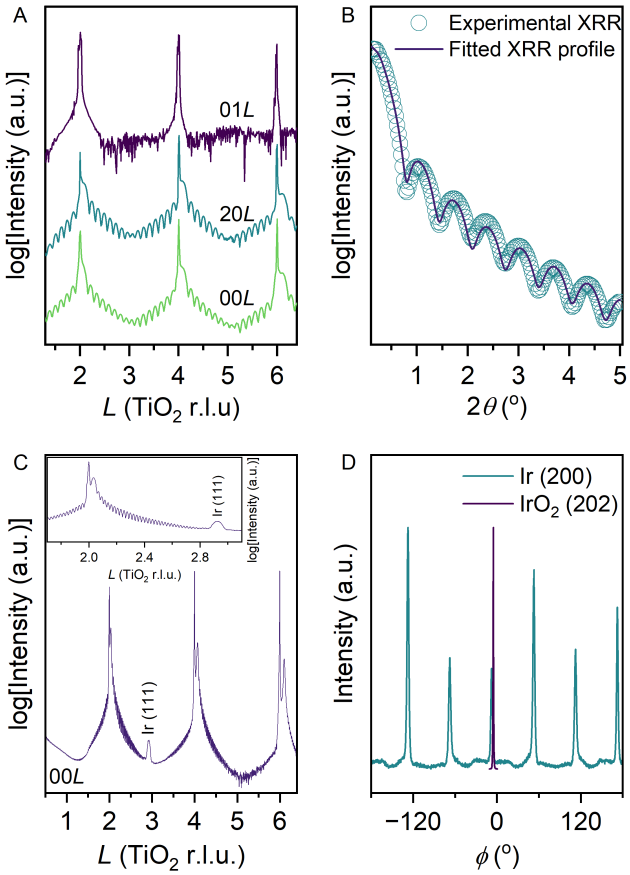

Figure S1: Synchrotron X-ray characterization of IrO_2 (110) films on TiO_2 (110) substrate. The peaks assigned for CTR scans and phi scans for IrO_2 only, are with respect to a redefined coordinate reference frame (indicated by *): a* = 6.487 Å (along TiO_2 [$1\bar{1}0$]), b* = 2.953 Å (along TiO_2 [001]), c* = 6.487 Å (along TiO_2 [110]. **(A)** Specular and off-specular CTR scans for a 5 nm IrO_2 (110) film. **(B)** XRR measurement for the same sample which shows well-defined Kiessig fringes indicative of a smooth film surface and sharp film-substrate interface. Solid line shows an algorithmic fit to the experimental data and the extracted surface roughness value is 1.073 ± 0.373 Å, attesting to the smooth film surface. **(C)** Specular CTR scan for a 26 nm IrO_2 (110) film. (Inset) CTR intensity for *L* between 1.7 and 3.1 reciprocal lattice units (r.l.u), which clearly shows presence of Laue oscillations even in the presence of Ir islands. **(D)** Phi scans about the (202) peak for IrO_2 and the (200) peak for Ir (face-centered cubic system). The intensities are normalized between [0,1] for better comparison, since the low sample volume of Ir led to low measured intensities compared to IrO_2. The phi scans reveal that the Ir (111) crystals are to a greater extent, aligned in plane with the epitaxial relation: Ir [$11\bar{2}$] ‖ IrO_2 [$1\bar{1}0$].

Figure S2:

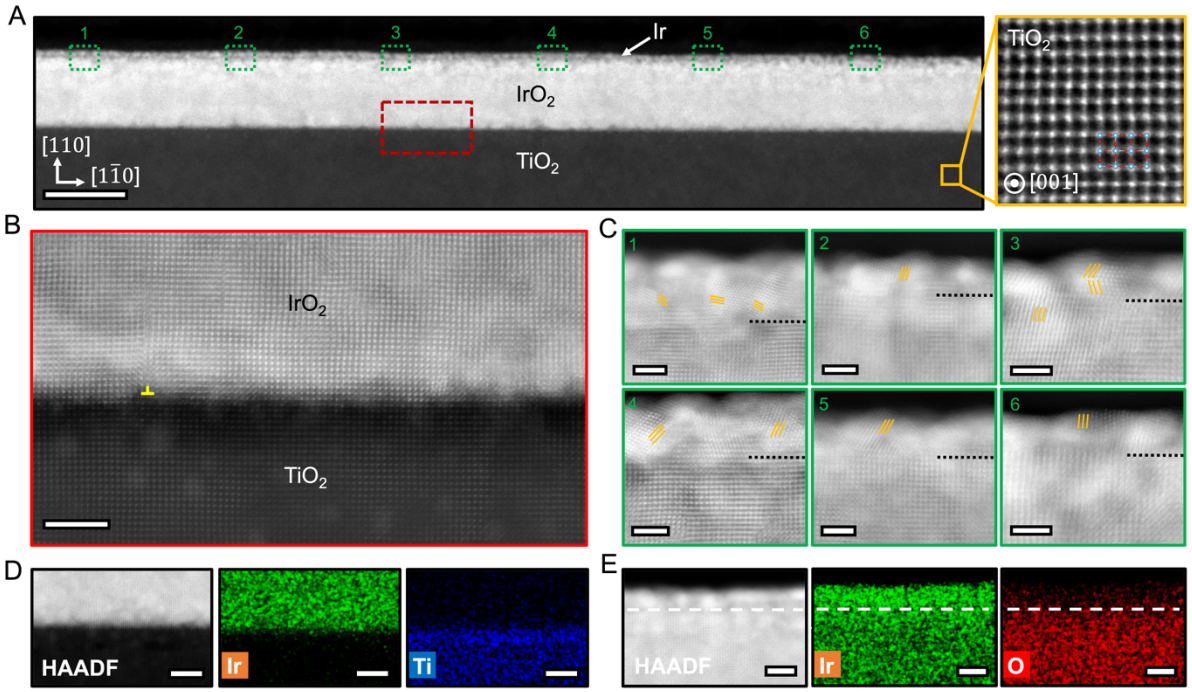

Figure S2: STEM images of a 21 nm IrO_2 (110) film on TiO_2 (110) substrate. **(A)** Low magnification STEM image of the Ir/IrO_2/TiO_2 structure. A ~2 nm highly textured Ir metal layer can be observed on top of IrO_2 showing different brightness contrast from the IrO_2 layer. Atomic resolution image of the TiO_2 substrate is shown on the right side. Scale bar = 25 nm. **(B)** Atomic resolution STEM image of the film-substrate interface showing sharp interface and presence of edge dislocations owing to the epitaxial misfit strain (ε = 2.23%). Scale bar = 3 nm. **(C)** Atomic resolution STEM images of the interface between the Ir particles and IrO_2 film. Lattices of neighboring Ir grains are indicated by yellow lines. The average measured spacing between the planes is ~ 2.26 Å, which matches with the expected (111) interplanar spacing for bulk face-centered cubic Ir crystal. Black dashed lines indicate the approximate interface position. Scale bar = 2 nm. **(D)** HAADF-STEM image of the IrO_2-TiO_2 interface and its complementary EDX elemental maps showing minimal elemental interdiffusion. Ir: green, Ti: blue. Scale bar = 5 nm. **(E)** HAADF-STEM image of the Ir and IrO_2 interface and its complementary EDX elemental maps where the surface Ir region shows reduced oxygen concentration. Ir: green, O: red. Scale bar = 3 nm. Dashed white line shows the approximate interface position between Ir and IrO_2.

Figure S3:

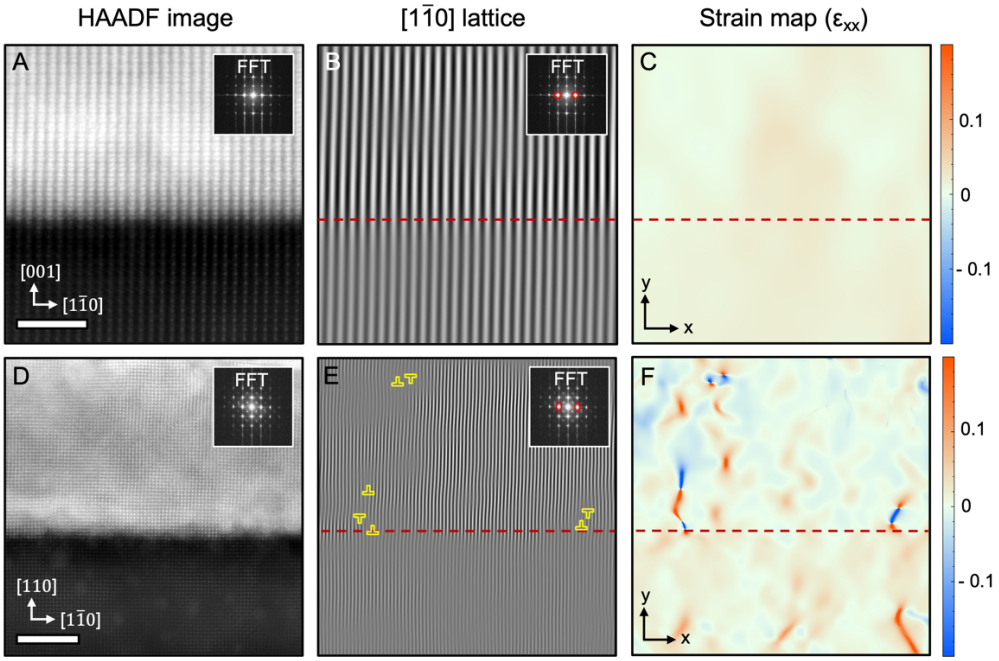

Figure S3: (A) HAADF-STEM image of IrO_2 (001) sample shown in Fig. 3C (scale bar = 2 nm). **(B)** [1$\bar{1}$0] lattice image constructed from inverse Fast Fourier Transform (FFT) in GPA analysis. **(C)** Strain map of the HAADF-STEM image in panel A, constructed using GPA. **(D)** HAADF-STEM image of IrO_2 (110) sample shown in Fig. S2B (scale bar = 5 nm). **(E, F)** Corresponding [1$\bar{1}$0] lattice image constructed from inverse FFT in GPA analysis and strain map constructed using GPA. A greater number of dislocations/dislocation pairs can be visualized in the [1$\bar{1}$0] lattice image which is difficult to elucidate in the HAADF-STEM image. Red dashed lines mark the film-substrate interface. Open yellow symbols represent edge dislocations. (insets to **(A, B, D, E)**) Diffraction patterns constructed using FFT; red circles indicate the diffraction spots used for reconstructing the lattice columns and strain maps.

Figure S4.

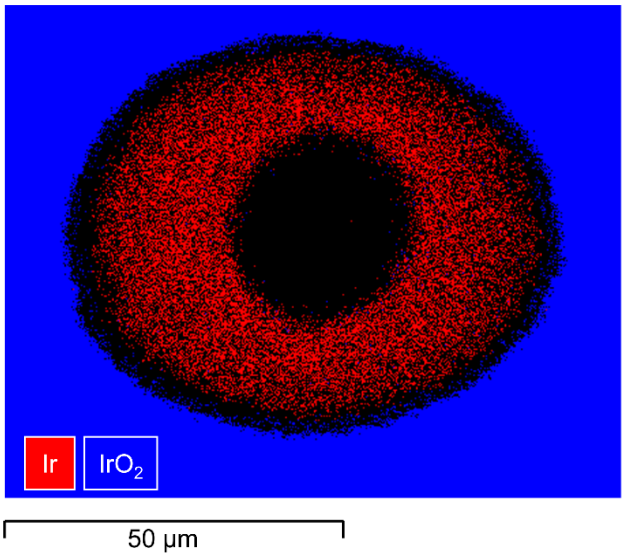

Figure S4: Electron Backscatter Diffraction (EBSD) map of a 23 nm IrO_2 (110) film containing surface Ir metal features grown on TiO_2 (110) substrate. An AZtecHKL software references the electron diffraction pattern with a pre-existing database to determine the best fit crystallographic plane. The map shows the IrO_2 (110) surface (blue) with Ir (111) crystals (red) present in the spot-like features. The black regions indicate unresolved regions and likely the presence of amorphous Ir metal.

Figure S5:

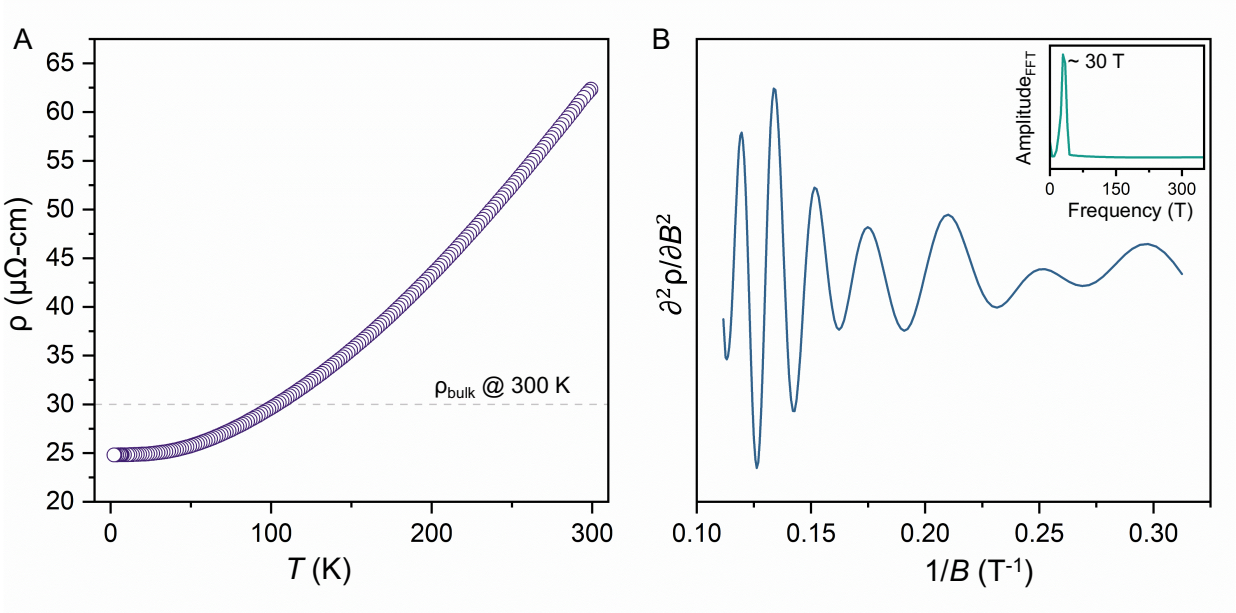

Figure S5: (A) Resistivity as a function of temperature for a 21 nm IrO_2 (110) film measured in a four probe Van der Pauw geometry using Al wire bonded electrical contacts. The dashed line shows the room temperature resistivity as reported for a bulk single crystal IrO_2[1]. **(B)** Second derivative of resistivity with respect to magnetic field at 2.5 K for a 13 nm IrO_2 (110) film, plotted against inverse magnetic field. The raw data for resistance as a function of magnetic field was smoothed using a Fast Fourier Transform (FFT) filter. (Inset) FFT amplitude of the oscillations in Fig. S5B plotted against frequency. Quantum oscillations in IrO_2 have only been reported in bulk-single crystals to date[2].

Figure S6.

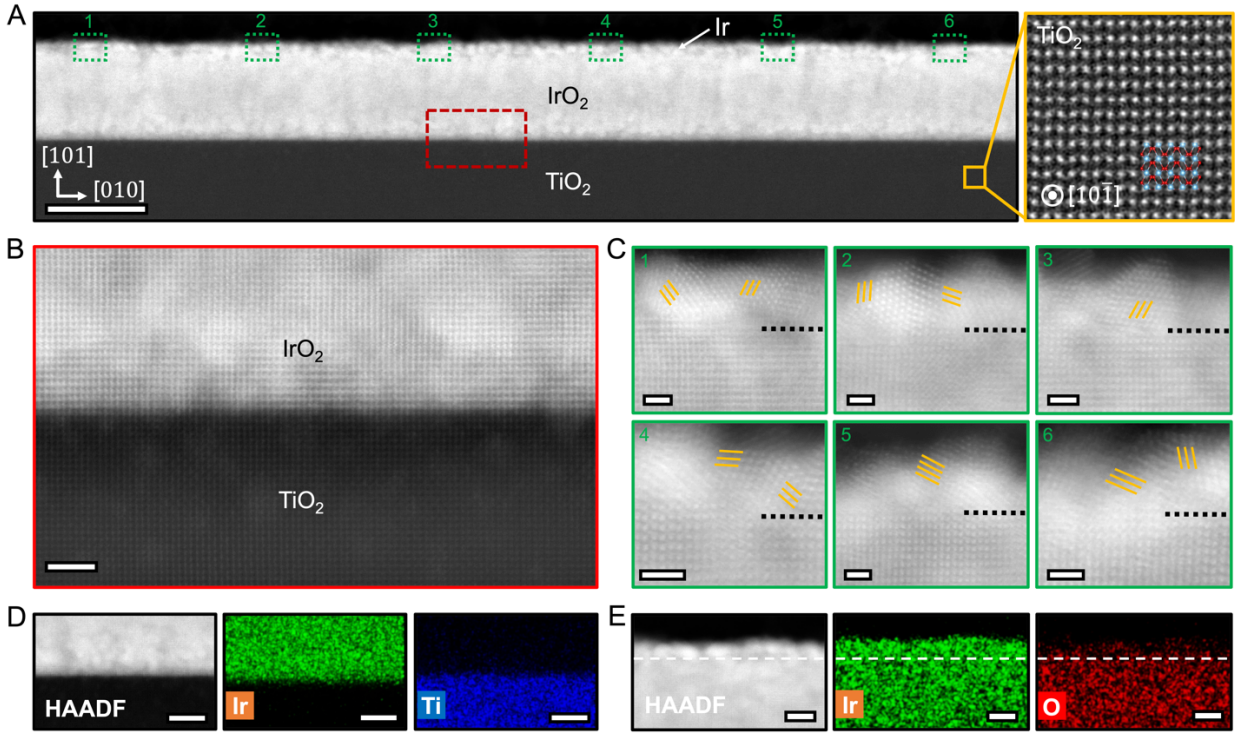

Figure S6: STEM characterization of a 22 nm IrO_2 (101) film on TiO_2 (101) substrate. **(A)** Low magnification STEM image of the Ir/IrO_2/TiO_2 structure. A ~2 nm polycrystalline Ir metal layer can be observed on top of the IrO_2 film showing different brightness from the IrO_2 layer. Atomic resolution image of the TiO_2 substrate is shown on the right side. Scale bar = 25 nm. **(B)** Atomic resolution STEM image showing epitaxially coherent IrO_2 film on the TiO_2 substrate (ε = -0.42%). Scale bar = 2nm. **(C)** Atomic resolution STEM images of the polycrystalline metal Ir and IrO_2 interface. Lattices of Ir neighboring grains are indicated by yellow lines. The average measured spacing between the planes is ~ 2.25 Å, close to the expected (111) interplanar spacing for bulk face-centered cubic Ir crystal. Black dashed lines indicate the approximate interface position. Scale bar = 1 nm. **(D)** HAADF-STEM image of the IrO_2-TiO_2 interface and its complementary EDX elemental maps showing sharp chemical profiles. Ir: green, Ti: blue. Scale bar = 5 nm. **(E)** HAADF-STEM image of the Ir-IrO_2 interface and its complementary EDX elemental maps showing reduced oxygen concentration in the Ir layer. Ir: green, O: red. Scale bar = 5 nm. Dashed white line demarcates the approximate interface position between Ir and IrO_2.

Figure S7.

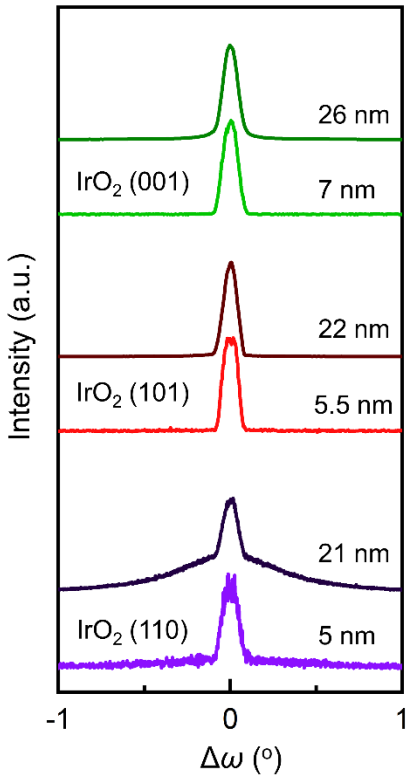

Figure S7: X-ray diffraction film rocking curves around the (220), (202) and (002) peaks of IrO_2 (110), IrO_2 (101) and IrO_2 (001) films of different thicknesses grown on corresponding TiO_2 substrates. The (101) and (001) films show similar full width maxima as a function of thickness in stark contrast to the thickness dependent emergence of broad component in the rocking curve for the IrO_2 (110) samples.

Figure S8:

A

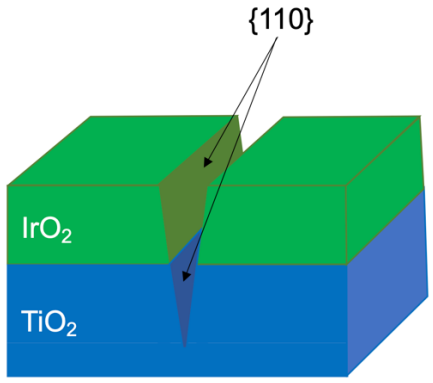

B

	{110} Surface Energy (J/m²)
IrO_2	1.68[3]
TiO_2	0.57[4]

Figure S8: (A) Schematic showing crack propagation from the IrO_2 film into the TiO_2 substrate along the {110} cleavage plane. **(B)** Surface energy values reported in literature for {110} family of planes of IrO_2 and TiO_2 respectively. The lower surface energy of the TiO_2 cleavage plane can provide an energetic compensation for crack propagation into the substrate. However, the exact mechanism and cause of film cracking and propagation would depend on additional factors like interfacial coupling, crack resistance of the film and substrate materials and other factors.

Figure S9:

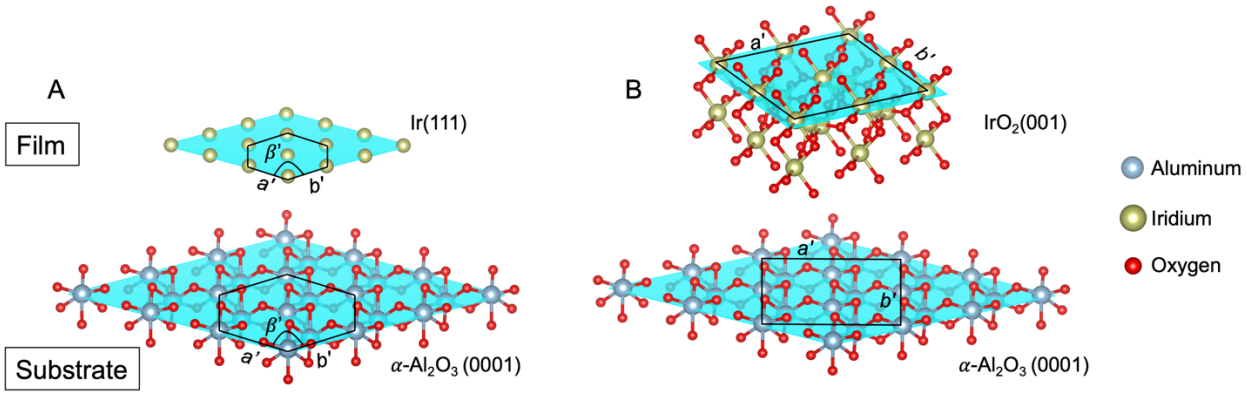

C

	Ir (111)	Ir(111)-epi	% strain
a'	2.714 Å	2.805 Å	3.37
b'	2.714 Å	2.805 Å	3.37
c'	6.648 Å	6.491 Å	-2.36
β'	120°	117.05°	

D

	IrO_2(001)	IrO_2(001)-epi	% strain
a'	9.010 Å	9.570 Å	6.22
b'	9.010 Å	8.288 Å	-8.02
c'	3.159 Å	3.167 Å	0.26
α', β', γ'	90°	90°	

Figure S9: Ball and stick models showing the preferred epitaxial relationship between **(A)** Ir metal and **(B)** IrO_2 films when grow on α-Al_2O_3 (0001) substrate. Change in lattice parameters and corresponding epitaxial strain values when (C) Ir (111) and (D) IrO_2 (001), (which are the most epitaxially preferred orientations on α-Al_2O_3 (0001) substrate) are fully strained and epitaxially connected to the substrate. ['epi' in (C, D) refers to the film when epitaxially strained by the substrate; *a', b', c', α', β', γ'* denote the lattice parameters for the unit cell in the transformed coordinate system defined for each out of plane crystal orientation; the terminology remains consistent for figures S10-S12 as well]

Ball and stick models for epitaxial strain calculations for Ir and IrO_2 films on TiO_2 substrates:

Figures S10-S12:

Figure S10-1

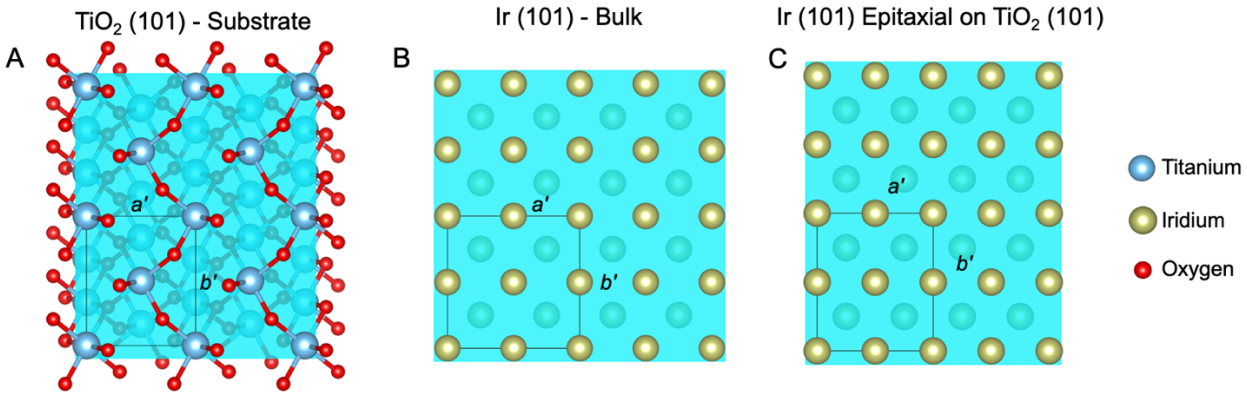

D

	TiO_2(101)
a'	4.594 Å
b'	5.464 Å

E

	Ir (101)	Ir (101)-epi	% strain
a'	5.428 Å	4.594 Å	-15.4
b'	5.428 Å	5.464 Å	0.67
c'	3.838 Å	4.280 Å	10.9
α', *β'*, *γ'*	90°	90°	

Figure S10-1: Ball and stick models showing the surface structure of **(A)** TiO_2 (101) substrate and preferred epitaxial orientation of Ir metal **(B)** in the bulk state and **(C)** in the epitaxially strained state. Lattice parameters for **(D)** TiO_2 (101) substrate and **(E)** comparison between bulk and epitaxial Ir (101) films and corresponding epitaxial strain values

Figure S10-2

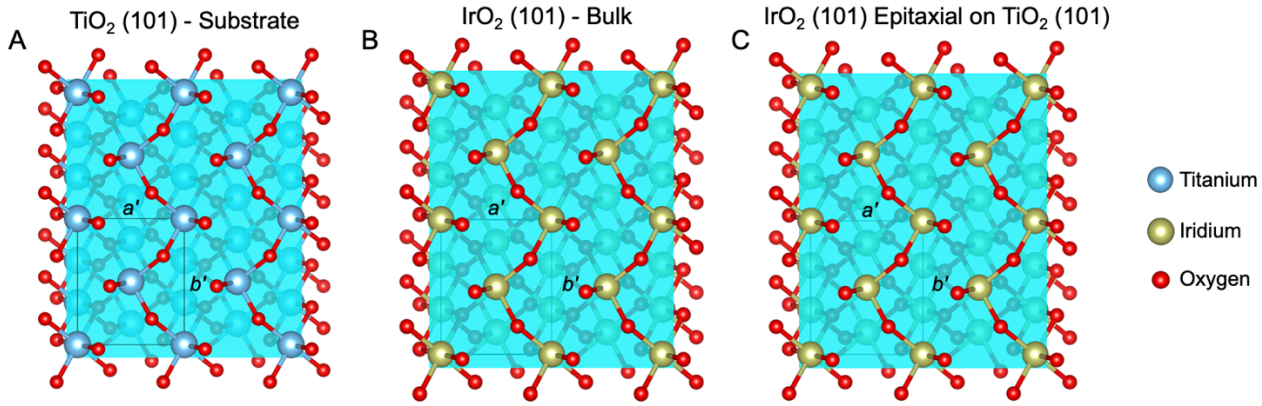

D

	TiO_2(101)
a′	4.594 Å
b′	5.464 Å

E

	IrO_2(101)-bulk	IrO_2(101)-epi	% strain
a′	4.505 Å	4.594 Å	-1.98
b′	5.502 Å	5.464 Å	0.69
c′	7.790 Å	7.878 Å	-0.60
α′, *β′*, *γ′*	90°	90°	

Figure S10-2: Ball and stick models showing the surface structure of **(A)** TiO_2 (101) substrate and preferred epitaxial orientation of IrO_2 **(B)** in the bulk state and **(C)** in the epitaxially strained state. Lattice parameters for **(D)** TiO_2 (101) substrate and **(E)** comparison between bulk and epitaxial IrO_2 (101) films and corresponding epitaxial strain values

Figure S11-1

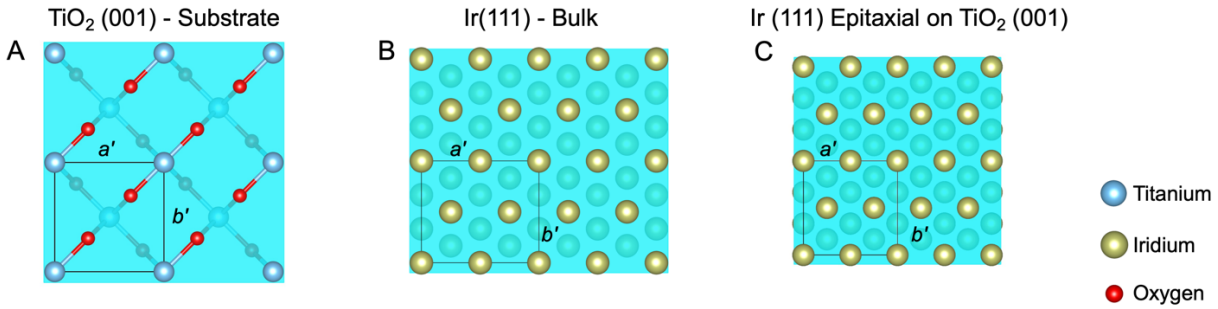

D

	TiO_2(001)
a'	4.594 Å
b'	4.594 Å

E

	Ir (111)	Ir (111)-epi	% strain
a'	5.428 Å	4.594 Å	-15.4
b'	4.701 Å	4.594 Å	-2.27
c'	6.628 Å	7.235 Å	7.85
α', *β'*, *γ'*	90°	90°	

Figure S11-1: Ball and stick models showing the surface structure of **(A)** TiO_2 (001) substrate and preferred epitaxial orientation of Ir metal **(B)** in the bulk state and **(C)** in the epitaxially strained state. Lattice parameters for **(D)** TiO_2 (001) substrate and **(E)** comparison between bulk and epitaxial Ir (111) films and corresponding epitaxial strain value

Figure S11-2

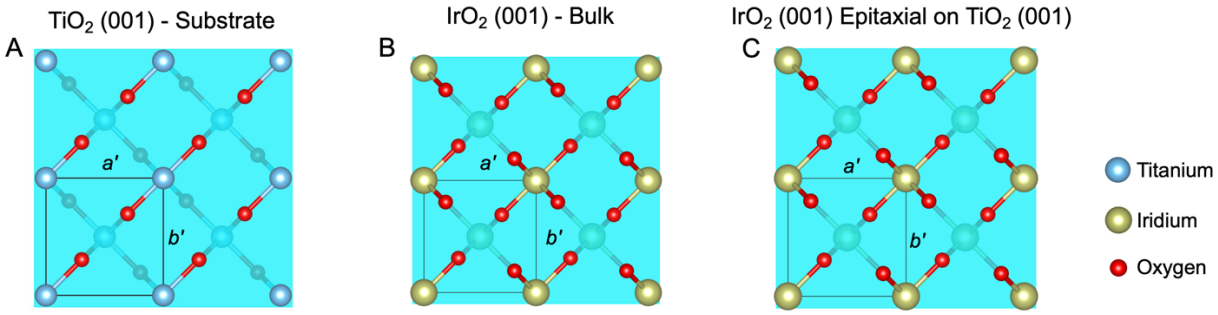

D

	TiO_2(001)
a'	4.594 Å
b'	4.594 Å

E

	IrO_2(001)	IrO_2(001)-epi	% strain
a'	4.505 Å	4.594 Å	1.98
b'	4.505 Å	4.594 Å	1.98
c'	3.159 Å	3.122 Å	-1.16
α', *β'*, *γ'*	90°	90°	

Figure S11-2: Ball and stick models showing the surface structure of **(A)** TiO_2 (001) substrate and preferred epitaxial orientation of IrO_2 **(B)** in the bulk state and **(C)** in the epitaxially strained state. Lattice parameters for **(D)** TiO_2 (001) substrate and **(E)** comparison between bulk and epitaxial IrO_2 (001) films and corresponding epitaxial strain values.

Figure S12-1

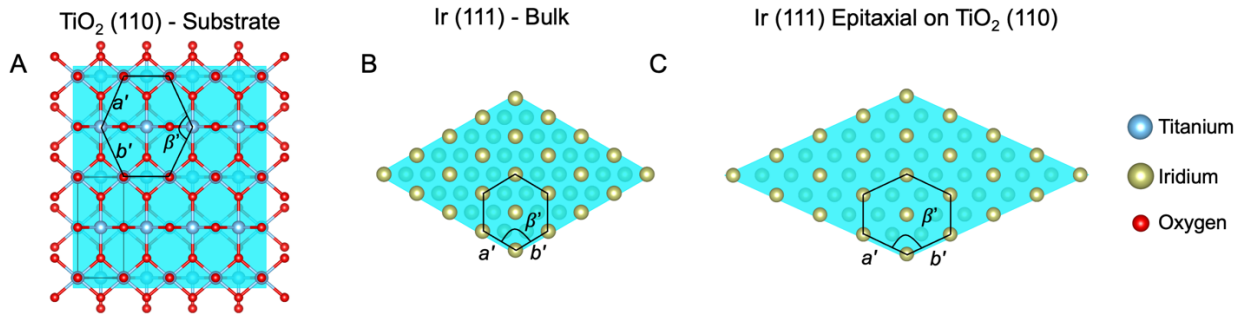

D

	TiO_2(110)
a′	3.570 Å
b′	3.570 Å
β′	131.03°

E

	Ir(111)	Ir(111)-epi	% strain
a′	2.714 Å	3.570 Å	+32
b′	2.714 Å	3.570 Å	+32
β′	120°	131.03°	

Figure S12-1: Ball and stick models showing the surface structure of **(A)** TiO_2 (110) substrate and preferred epitaxial orientation of Ir **(B)** in the bulk state and **(C)** in the epitaxially strained state. Lattice parameters for **(D)** TiO_2 (110) substrate and **(E)** comparison between bulk and epitaxial Ir (111) films and corresponding epitaxial strain values.

Figure S12-2

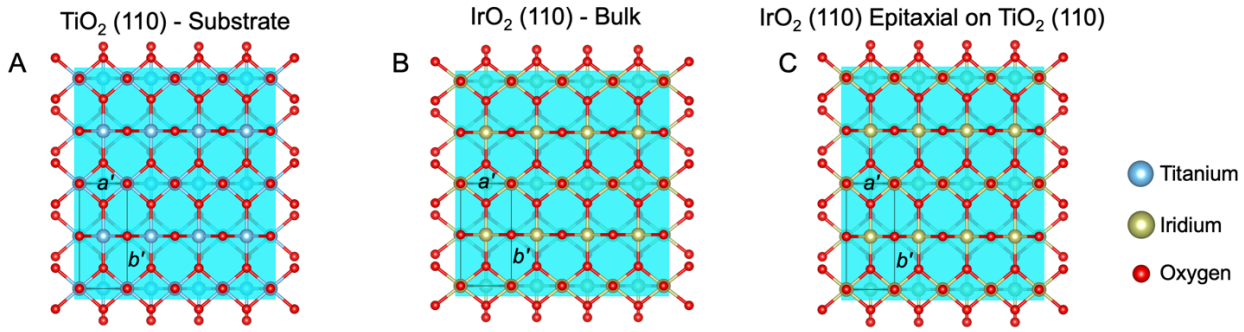

D

	TiO_2(110)
a'	2.959 Å
b'	6.497 Å

E

	IrO_2(110)	IrO_2(110)-epi	% strain
a'	3.159 Å	2.959 Å	-6.33
b'	6.371 Å	6.497 Å	1.98
c'	6.371 Å	6.543 Å	2.71
α', *β'*, *γ'*	90°	90°	

Figure S12-2: Ball and stick models showing the surface structure of **(A)** TiO_2 (110) substrate and preferred epitaxial orientation of IrO_2 **(B)** in the bulk state and **(C)** in the epitaxially strained state. Lattice parameters for **(D)** TiO_2 (110) substrate and **(E)** comparison between bulk and epitaxial IrO_2 (110) films and corresponding epitaxial strain values.

Figure S13.

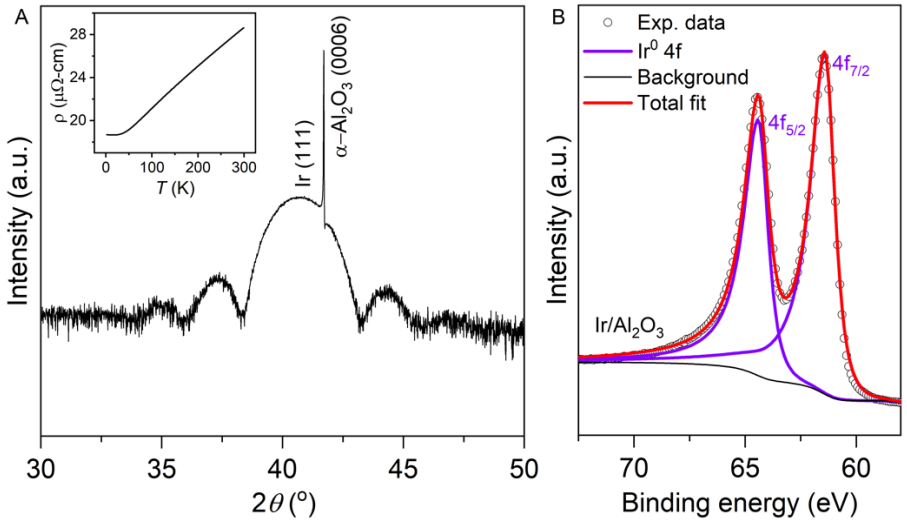

Figure S13: (A) XRD 2θ - ω coupled scans showing phase-pure single crystalline Ir metal on *c*-sapphire substrate. (inset) Resistivity as a function of temperature measured in the Van der Pauw geometry showing metallic behavior. **(B)** Experimental XPS data and peak fits for the Ir 4f core level showing the elemental metal state.

Figure S14.

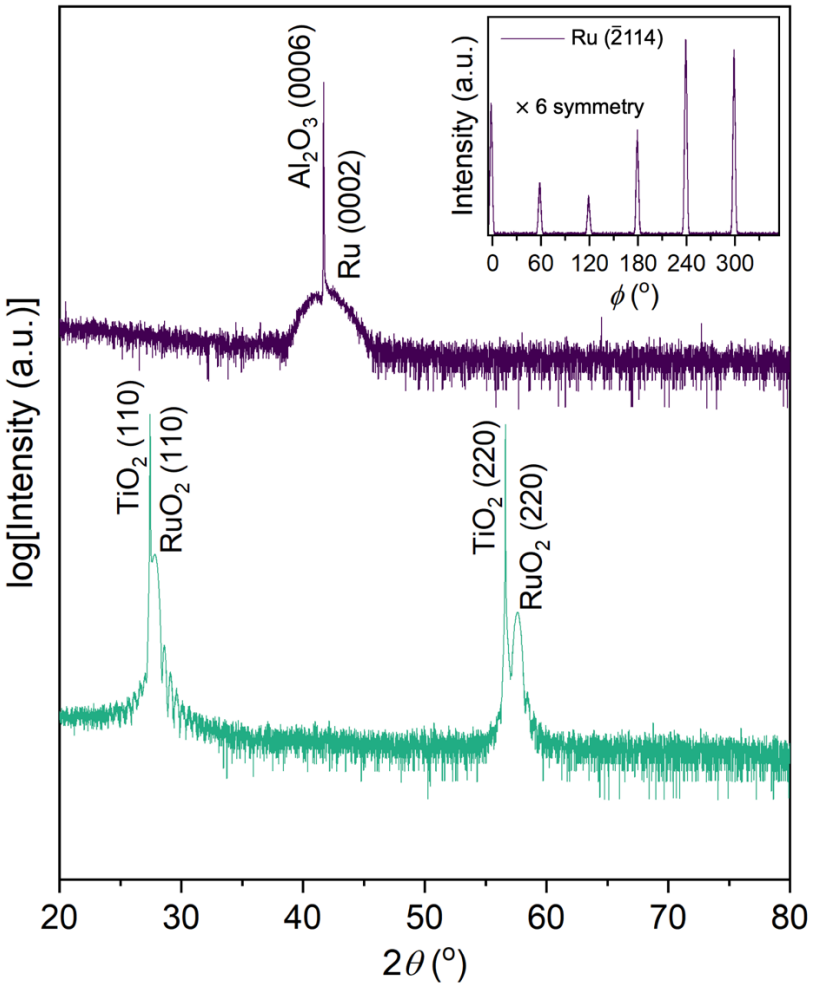

Figure S14: XRD 2θ - ω coupled scans for as grown RuO_2 (110) film grown on TiO_2 (110) substrate and Ru (0001) film grown on *c*-Al_2O_3 substrate, both at a substrate temperature of 300 °C and oxygen pressure of 5×10^{-6} Torr. (inset) XRD phi scans about the asymmetric ($\bar{2}$114) peak for hcp Ru showing the expected six-fold symmetry confirming the formation of Ru metal even under strong oxidizing condition.

Figure S15.

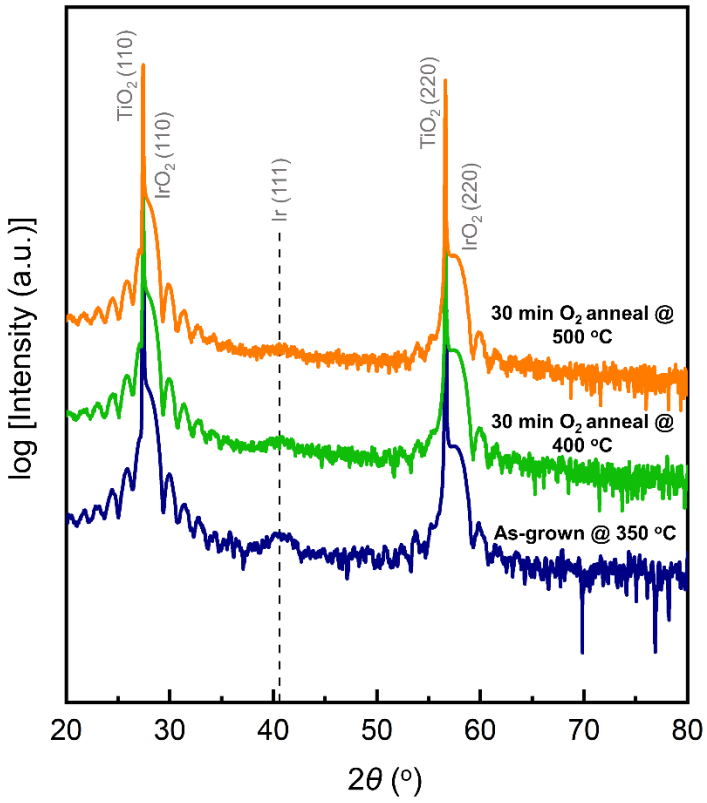

Figure S15: XRD 2θ - ω coupled scans for as grown IrO_2 (110) film grown at 350 °C substrate temperature and after 30 minutes of ex-situ oxygen annealing at 400°C and 500 °C respectively.

References:

1 Butler, S. R. & Gillson, J. L. Crystal Growth, Electrical Resistivity and Lattice Parameters of Ruo2 and Iro2. *Mater Res Bull* **6**, 81-&, doi:Doi 10.1016/0025-5408(71)90092-4 (1971).

2 Ryden, W. D., Reed, W. A. & Greiner, E. S. High-Field Magnetoresistance of IrO2. *Physical Review B* **6**, 2089-2093, doi:10.1103/PhysRevB.6.2089 (1972).

3 Matz, O. & Calatayud, M. Periodic DFT Study of Rutile IrO2: Surface Reactivity and Catechol Adsorption. *The Journal of Physical Chemistry C* **121**, 13135-13143, doi:10.1021/acs.jpcc.7b01990 (2017).

4 Zheng, T., Wu, C., Chen, M., Zhang, Y. & Cummings, P. T. A DFT study of water adsorption on rutile TiO2 (110) surface: The effects of surface steps. *The Journal of Chemical Physics* **145**, 044702, doi:10.1063/1.4958969 (2016).